Nanoscale

PAPER

View Article Online
View Journal | View Issue

Cite this: *Nanoscale*, 2024, **16**, 2993

Cooperative dissolution of peptidomimetic vesicles and amyloid β fibrils†‡

Soumik Dinda, Debasis Ghosh and Thimmaiah Govindaraju *

Received 25th September 2023,
Accepted 4th January 2024

DOI: 10.1039/d3nr04847k

rsc.li/nanoscale

The aggregation of amyloid proteins in the brain is a significant neurotoxic event that contributes to neurodegenerative disorders. The aggregation of amyloid beta (Aβ), particularly Aβ42 monomers, into various forms such as oligomers, protofibrils, fibrils, and amyloid plaques is a key pathological feature in Alzheimer's disease. As a result, Aβ42 is a primary target and the development of molecular strategies for the dissolution of Aβ42 aggregates is considered a promising approach to mitigating Alzheimer's disease pathology. A set of pyrene-conjugated peptidomimetics derived from Aβ14-23 (Akd^{c}Py, Akd^{m}Py, and Akd^{n}Py) by incorporating an unnatural amino acid [kd: cyclo(Lys-Asp)] were studied for their ability to modulate Aβ42 aggregation. Akd^{c}Py and Akd^{m}Py formed vesicular structures in aqueous media. The vesicles of Akd^{m}Py loaded with the neuroprotective compound berberine (Ber), dissipated mutually in the presence of preformed Aβ42 fibrils. During this process, the active drug Ber was released. This work is expected to inspire the development of drug-loaded peptidomimetic-based therapeutic formulations to modulate disorders associated with amyloid toxicity.

Introduction

The scheme of molecular architectonics allows for the creation of smart molecular architectures with customized size, shape, properties, and functions.[1–7] In recent years, there has been a surge in research activity focused on developing designer molecular architectures using amphiphiles with variable structural motifs.[8–10] Vesicles, in particular, have garnered significant attention due to their unique hollow microstructure, cell penetrability, retention ability, and potential for a wide range of applications including bio-catalysis and bio-medicines.[11–13] The vesicles formed from small molecules exhibit unique dynamic behaviour and are typically formed through the aggregation of amphiphiles held together by noncovalent interactions such as hydrogen bonding, hydrophobic interactions, van der Waals forces, and π–π stacking.[14–18] The molecular aggregation can be manipulated in response to external stimuli.[19–21] By incorporating stimuli-responsive moieties into the building blocks, it is possible to create smart vesicles that can respond to changes in their physico-chemical environment. The development of vesicular architectures with high cargo loading capacity and precise responsiveness to specific targets would be highly advantageous. One potential application could be the targeted modulation of biologically toxic protein aggregates as in Alzheimer's disease (AD), which is caused by the accumulation and deposition of amyloid beta (Aβ) aggregates in the brain.[22–26]

Currently, approximately 50 million people worldwide are suffering from AD, and this figure is expected to exceed 130 million by 2050.[27,28] Despite substantial progress in understanding the mechanistic pathway underlying AD,[29–33] there remains an urgent need to identify effective modalities to address this serious public health problem. One characteristic of AD is the generation of abnormal Aβ peptides (37–43 amino acids) through irregular proteolytic cleavage of the amyloid precursor protein (APP).[34,35] In particular, Aβ42 undergo aggregation to form oligomers, protofibrils, fibrils, and insoluble plaques in the extracellular regions of the brain, which is the major culprit in AD pathology.[22] The surface of mature fibrils acts as an active catalytic surface that produces highly toxic Aβ oligomeric species.[22] While removal of brain-Aβ using Aβ-specific antibodies is a common approach, it is associated with autoimmunity-related adverse side effects.[36] Peptidomimetic candidates have been identified as a suitable alternative for modulating Aβ fibrillation.[37–39] The inorganic based materials like graphene oxide and silicene nanosheets have also been employed for the irreversible disassembly of Aβ aggregates.[40,41] Although numerous molecular strategies to inhibit Aβ42 aggregation are reported, the dissolution of preformed aggregates is a crucial and challenging task. Therefore,

Bioorganic Chemistry Laboratory, New Chemistry Unit and School of Advanced Materials (SAMat), Jawaharlal Nehru Centre for Advanced Scientific Research (JNCASR), Jakkur P.O., Bengaluru 560064, Karnataka, India.
E-mail: tgraju@jncasr.ac.in

† Dedicated to Professor Santanu Bhattacharya on his 65th birthday.

‡ Electronic supplementary information (ESI) available. See DOI: https://doi.org/10.1039/d3nr04847k

the development of new peptidomimetic-based smart architectures that can facilitate drug delivery and modulate aggregation of preformed Aβ aggregates may represent an innovative therapeutic approach for the treatment of AD.

In this study, we report the design and synthesis of a set of pyrene-conjugated Aβ14-23 peptidomimetics ($Akd^{c}Py$, $Akd^{m}Py$, and $Akd^{n}Py$) incorporated with unnatural amino acid [kd: cyclo(Lys-Asp)] at pre-determined positions, C-terminal (c), middle (m) and N-terminal (n), respectively. The rigid, proteolytically stable, and biocompatible kd unit was considered for its ability to form hydrogen bonding interactions, while the pyrene residue imparts π–π stacking and hydrophobic interactions.[8,42] Among these, $Akd^{c}Py$ and $Akd^{m}Py$ spontaneously formed vesicles in aqueous media. The physicochemical characterizations of these synthesized vesicles were performed using various microscopy and spectroscopy techniques. Surprisingly, it was observed that the vesicles of $Akd^{m}Py$ dissipated in the presence of preformed Aβ42 fibrils, which subsequently aided in the dissolution of the later. The vesicles exhibited high specificity towards toxic Aβ42 compared to other biologically relevant molecules (carbohydrates, proteins, and essential metal ions). Furthermore, the vesicles were successfully loaded with the neuroprotective drug berberine (Ber). Ber is an isoquinoline alkaloid and a well-known ingredient of Chinese medicine that has the potential to interfere with the pathological pathways of AD.[43,44] It also delays oxidative stress, enhances gliosis, prevents neuroinflammation, and inhibits secretase enzymes involved in APP processing, all of which contribute to reducing Aβ toxicity.[43] The Ber-loaded vesicles have greater potential due to their synergistic effect compared to the individual drug (Ber) or carrier ($Akd^{m}Py$). To the best of our knowledge, this is also a unique approach to employ drug-loaded vesicles for the dissolution of preformed Aβ42 fibrils. It is anticipated that the release of the neuroprotective medication following the disintegration of the Ber-loaded vesicle in the presence of Aβ42 peptide will result in greater mitigation against amyloidosis in Alzheimer's and other diseases with improved clinical outcomes.

Experimental section

Materials and methods

All solvents and reagents were purchased from Spectrochem or Merck and utilized without further purification unless otherwise mentioned. Distilled water (0.055 μS Cm^{-1}) was used throughout the entire study. Sephadex-G25 and Rhodamine B (RhB), berberine chloride (Ber) were purchased from Sigma Aldrich. 1,6-Diphenyl-1,3,5-hexatriene (DPH) dye, were procured from TCI Chemicals (India) Pvt., Ltd. Heat-inactivated fetal bovine serum (FBS) was obtained from Invitrogen. Bath sonication was performed in an Elmasonic (ultrasonic) bath sonicator. ^{1}H NMR spectra were recorded on Bruker AV-400 and JEOL-600 MHz spectrometers using tetramethylsilane (TMS) as the internal standard. Agilent 6538 UHD HRMS/Q-TOF high-resolution spectrometer was utilized to acquire High-resolution mass spectra. MALDI-TOF data was acquired in Bruker Autoflex Speed MALDI TOF spectrometer. Fluorescence imaging was carried out in a Leica DMi8 fluorescence microscope, and the images were processed with Huygens software.

Synthetic procedure for peptidomimetic amphiphiles

The synthesis of all peptidomimetics was performed using established solid phase peptide synthesis (SPPS) procedures with Fmoc-rink amide resin as the solid support.[42] Amino acids and unnatural CDP-amino acid (kd) were coupled using HBTU/HOBt as the activating reagent and DIPEA as the base in DMF. Fmoc deprotection was achieved using 20% piperidine in DMF (Scheme S1‡). Purification of the peptides was carried out using reverse-phase semi-preparative HPLC with a C18 column at 40 °C, resulting in a product purity of >99% as verified by analytical HPLC (Table S1‡). The molecular mass of the peptides was confirmed by HRMS (Q-TOF) analysis (Table S2‡). The sequence and structural data for the kd-containing peptidomimetics synthesized are presented in Table S1 and S2.‡

Preparation of vesicles

All of the amphiphiles ($Akd^{n}Py$, $Akd^{m}Py$, and $Akd^{c}Py$) were found to be soluble in aqueous conditions (0.5 mg mL^{-1}). However, $Akd^{n}Py$ was not so stable in water, and it was precipitated out immediately. Hence, $Akd^{m}Py$ and $Akd^{c}Py$ (1 mg) was dissolved in distilled water (2 mL) in two separate vials to form the translucent solution of the desired architecture. All the microscopy and spectroscopy characterizations were performed with these solutions.

Critical aggregation concentration (CAC)

The critical aggregation concentration (CAC) for both amphiphiles ($Akd^{m}Py$ and $Akd^{c}Py$) was determined by static light scattering (SLS) measurements on a luminescence spectrometer.[45] Stock solutions of $Akd^{m}Py$ and $Akd^{c}Py$ were prepared (300 μM) in distilled water and the scattering intensities were measured upon successive dilutions. The excitation wavelength remained at a fixed λ = 340 nm and the slit width was set at 5 nm during the measurement of scattered light intensity. The scattered intensities were plotted against the concentrations and the CAC value for each amphiphile was determined from the inflection point of each plot.

Transmission electron microscopy (TEM)

In this study, 3 μL of the $Akd^{m}Py$ and $Akd^{c}Py$ aqueous solution (100 μM) were drop cast separately onto carbon-coated copper grids, left to adsorb for 1 minute, and excess solution was removed by blotting paper. The grids were then negatively stained with a 1 μL aqueous solution of freshly prepared uranyl acetate (1% w/v) and the excess solution was also removed by blotting paper. Subsequently, the grids were dried for 5 hours under vacuum and analyzed in a JEOL JEM 3010 TEM.

In a separate experiment, the pre-incubated Aβ42 fibril (10 μM) in the absence and presence of $Akd^{m}Py$ with varying concentrations (25–80 μM) were placed on a carbon-coated

copper grid of 200 mesh and negatively stained with freshly prepared (1% w/v) uranyl acetate. The grids were kept for 5 h under vacuum for drying before the experiment. In another investigation, TEM was used to analyze the effect of Akd^{m}Py vesicle (40 μM) on the preformed Aβ42 fibrils (10 μM) over different time intervals (5 min–48 h). The grids were prepared according to a similar procedure as stated previously. The effectiveness of the drug-loaded vesicle was also evaluated through TEM analysis of Aβ42 fibril (10 μM) incubated for 1 h with Ber (10 μM), Akd^{m}Py vesicle (40 μM), and Ber-loaded Akd^{m}Py vesicle.

Field-emission scanning electron microscopy (FESEM)

FESEM experiment was performed in a FEL Nova nanoSEM-600 equipped with a 15 kV field emission gun and a Quanta CD FEG at 20 kV. 6 μL of Akd^{m}Py and Akd^{c}Py aqueous solutions (100 μM) were placed separately on the pieces of silicon wafer and dried overnight. Samples were kept few hours under vacuum before imaging.

Atomic force microscopy (AFM)

The aqueous solution of Akd^{m}Py and Akd^{c}Py (100 μM) was drop cast separately on freshly cleaved mica discs. The samples were kept undisturbed for 15 min under room temperature, washed with 0.22 micron filtered distilled water thrice for 5 min, and dried for 30 min at 37 °C. The AFM experiment was performed in a Bruker BIOSCOPE Resolve with PeakForce Tapping AFM instrument. All the AFM data were processed and analyzed by NanoScope 1.8 analysis software (Bruker).

In a separate experiment, the pre-incubated Aβ14-23 peptide (10 μM) in the absence and presence of Akd^{m}Py vesicle with varying concentrations (25 μM, 40 μM, and 80 μM) were placed on freshly cleaved mica discs and dried in a similar way before the experiment.

Dynamic light scattering (DLS)

The mean hydrodynamic diameters of the molecular assembly architectures were ascertained by DLS measurement using a fixed-angle apparatus, namely the ZetaPALS, Zeta Potential Analyzer (Brookhaven Instruments Corporation, USA). Solutions of Akd^{m}Py and Akd^{c}Py over a varying concentrations range (40–500 μM) were prepared in an aqueous medium. The acquired scattering intensity data with distinct solution concentrations were processed through a data processor equipped with specific software. Each sample underwent three sequential measurements, and their average values were computed.

Fluorescence anisotropy

Fluorescence anisotropy values were determined in an Agilent Cary Eclipse fluorescence spectrophotometer where 1,6-diphenyl-1,3,5-hexatriene (DPH) was used as a hydrophobic fluorescent probe. The steady-state anisotropy (r) of DPH was measured in individual aqueous solutions of Akd^{m}Py and Akd^{c}Py with varying concentrations (40–500 μM). A stock solution of DPH (0.2 mM) was prepared in tetrahydrofuran (THF), and the final concentration of DPH was maintained at 1 μM in each solution. The DPH dopped Akd^{m}Py and Akd^{c}Py in water were excited at λ = 370 nm. The emission intensity was recorded at λ = 450 nm using an emission cut-off filter at λ = 430 nm to avoid any scattering due to turbidity of the solution. The slit widths for excitation and emission were kept at 5 nm. The fluorescence anisotropy value (r) was determined by the instrumental software using following eqn (1).[18,46]

$$r = (I_{VV}\text{-}GI_{VH})/(I_{VV} + 2GI_{VH}) \quad (1)$$

Here, the intensities of emission spectra were obtained with vertical and horizontal polarization for vertically polarized light, denoted as I_{VV} and I_{VH}, respectively. The instrumental correction factor, denoted as G, was calculated as I_{HV}/I_{HH}, where I_{HV} and I_{HH} are the emission intensities obtained with vertical and horizontal polarization for horizontally polarized light, respectively. The measurements were carried out a minimum of five times for each sample at a temperature of 25 °C

UV-vis study

To determine the aggregation pattern of Akd^{m}Py and Akd^{c}Py, UV-vis spectroscopy study was carried out. The solvent-dependent UV-vis spectra of Akd^{m}Py and Akd^{c}Py were recorded in an Agilent Cary series UV-vis-NIR spectrophotometer. Different solvent systems were used, ranging from DMSO (molecularly dissolved state) to water (molecularly assembled state). DMSO–H_2O (1 : 1 v/v) was selected as an intermediate solvent. The concentrations of amphiphilic molecules (Akd^{m}Py and Akd^{c}Py) were set at 50 μM to record the absorbance.

Solvent dependent ^{1}H NMR measurements

Solvent dependent ^{1}H NMR spectra of Akd^{m}Py and Akd^{c}Py were recorded in a Bruker AV-400 spectrometer where the compound concentrations were fixed at 0.3 mg mL^{-1}. The solvents were varied form [D_6]DMSO (non-self-aggregating solvent) to D_2O (self-aggregating solvent) for both amphiphiles. [D_6]DMSO-D_2O (1 : 1 v/v) was chosen as a mixed solvent in between the two extreme solvent systems.

Dye entrapment and release study

Both the amphiphiles, Akd^{m}Py and Akd^{c}Py (1 mg each), was mixed with 40 μL of RhB (1 mM) solution in water in two separate vials and the volume was made up to 1 mL for each vial with distilled water. The final concentrations of amphiphile and RhB were 588 μM (1 mg mL^{-1}) and 40 μM, respectively and it was kept overnight under stirring condition. Each solution was then loaded into two separate sephadex G-25 column (12 cm height and 1.2 cm diameter) pre-equilibrated with distilled water and eluted with the same. Vesicular solutions were eluted immediately following the void volume. The filtration process was repeated until all un-entrapped RhB was gel-filtered and eliminated completely. The eluent was collected in a 2 mL fraction. To confirm the existence of RhB in each fraction, the absorbance of each fraction was measured at 554 nm. Eluent was collected until there was no measurable absorbance of RhB. Finally, Triton X-100 (0.5% (v/v)) was applied to

the vesicles to rupture them and determine the amount of dye loaded.[18] Percentage loading of the dye was determined from the standard calibration curve of RhB. The loading of RhB within vesicles was further ensured from the comparison studies of fluorescence intensity of only RhB and entrapped RhB within both the vesicles at λ_{em} = 578 nm (λ_{ex} = 545 nm). For release experiments, Triton X-100 (0.5% (v/v)) was added to the dye loaded vesicular solution of both Akd^{m}Py and Akd^{c}Py and the fluorescence spectra were recorded. Both solutions before and after Triton X-100 treatment were further examined in a fluorescence microscope.

Ber loading in Akd^{m}Py vesicles

Neuroprotective drug Ber was loaded in Akd^{m}Py vesicles in a conventional thin film hydration technique. In a typical experiment, Akd^{m}Py (1 mg) and Ber (1 mg) were placed in a round-bottomed flask. 5 mL of methanol was added to make all of the components soluble completely, and the mixture was stirred for 6 h. Methanol was then evaporated in a rotary evaporator at 45 °C to generate a thin film. Finally, the film was hydrated with 3 mL of distilled water and stirred for 1 h. The resulting solution was sonicated for 30 minutes to form a homogeneous vesicles entrapped with Ber. The unentrapped drug molecules were removed by a size exclusion column (12 cm height and 1.2 cm diameter) with sephadex G-25 pre-equilibrated with distilled water. Elution was carried out with distilled water and drug entrapped vesicular solution was collected in 2 mL fraction each. The absorbance for all the fractions was measured at λ = 375 nm to confirm the presence of Ber. Eluent was collected till no detectable absorbance of Ber was found. Finally, Triton X-100 (0.5% (v/v)) was used to rupture the drug loaded vesicles and estimate the percent of drug loading using a calibration curve. The drug loading capacity (%) was calculated using the following eqn (2).[47]

$$W_D/W_L \times 100 \quad (2)$$

where W_D is the amount of drug loaded inside the vesicle and W_L is the total amount of drug taken during the drug-loading experiment. The drug loaded vesicular fluid was investigated further in a fluorescence microscope. The Ber entrapped vesicular solution of Akd^{m}Py was treated with Triton X-100 (0.5% (v/v)) for drug release studies, and the fluorescence spectra were collected before and after the addition of Triton X-100.

Preparation of Aβ42 fibrils

Aβ42 peptide (100 μg) was dissolved completely in hexafluoro-2-propanol (HFIP, 250 μL) and incubated at room temperature for 1 h. After which the HFIP was eliminated through nitrogen gas. The processed Aβ42 peptide was then dissolved in 2% DMSO and PBS buffer (pH = 7.4) to create Aβ42 in a monomeric state, with its concentration being determined using absorption at 280 nm (ε = 1450 cm^{-1}M^{-1}). The resultant Aβ42 in monomeric form was subjected to prolonged incubation at 37 °C for 48 h in PBS buffer (pH = 7.4), resulting in the formation of Aβ42 fibrils.

Interaction of Akd^{m}Py vesicle with preformed Aβ42 fibrils

Various spectroscopy and microscopy techniques were used to investigate the interaction between Akd^{m}Py vesicles and preformed Aβ42 fibrils. Fluorescence spectra were obtained for Akd^{m}Py monomer and Akd^{m}Py vesicle. On the other hand, fluorescence spectra were recorded for Akd^{m}Py vesicles (40 μM) before and after incubation with preformed Aβ42 fibrils and Aβ42 monomer (10 μM). Additionally, dye and drug loaded Akd^{m}Py vesicles were treated with Aβ42 monomer and preformed Aβ42 fibrils (10 μM) and fluorescence spectra were recorded. DLS studies were conducted to evaluate the effect of preformed Aβ42 fibrils on the vesicular assembly. Preformed Aβ42 fibrils (10 μM) was added to the Akd^{m}Py vesicle solution (40 μM) and scattering data were collected before and after treatment.

Circular dichroism (CD) study

The changes in secondary structural conformations of Aβ42 fibril and Aβ14-23 fibril upon interaction with Akd^{m}Py vesicle were monitored by CD spectroscopy. To record the CD spectra, preformed Aβ42 and Aβ14-23 fibrils (10 μM) were incubated with solution containing Akd^{m}Py vesicles (40 μM) at 37 °C for 48 h in PBS buffer (pH = 7.4). The CD spectra, Aβ42 and Aβ14-23 fibrils (10 μM) were recorded as control. For a typical experiment, a quartz cuvette having path length of 0.1 cm was used, and the spectra were recorded in the wavelength range of λ = (190–240) nm at a 50 nm min^{-1} scan rate. For CD analyses, the background correction was performed using the CD spectrum recorded in only PBS buffer (pH = 7.4).

Specificity

The fluorescence spectra of Akd^{m}Py solution were recorded in absence and presence of biologically relevant species like glucose, sodium ascorbate, proteins (BSA, FBS) and essential metal ions (Na^+, K^+) to determine if synthesized vesicle (Akd^{m}Py) can specifically interact with Aβ42 fibrils. The concentration of Akd^{m}Py solution and each of the analytes were fixed at 40 μM and 10 μM, respectively, and the relative change in intensity of the fluorescence spectra was monitored.

Thioflavin T (ThT) fluorescence study

The disaggregation of the preformed Aβ42 fibrils in the presence and absence of the Akd^{m}Py was investigated by ThT fluorescence study. The preformed Aβ42 fibrils (10 μM) was incubated with Akd^{m}Py vesicle (40 μM) in the presence of ThT fluorescent dye (λ_{ex} = 442 nm and λ_{em} = 482 nm). ThT fluorescence was monitored in a time-dependent manner.

Aβ42 fibril responsive drug release profile

The present study aimed to investigate the Aβ42 fibril responsive drug release from Akd^{m}Py vesicles by monitoring the steady-state fluorescence spectrum under various experimental conditions. The percentage of released drug was estimated by calculating the relative fluorescence intensities at λ = 550 nm of the Ber-loaded vesicles before and after treatment with pre-

formed Aβ42 fibrils. A concentration-dependent drug release assay was conducted using Ber-loaded vesicles and different concentrations of preformed Aβ42 fibrils (1 to 50 μM). Additionally, a time-dependent drug release profile was examined by varying the incubation time (0 to 15 min) of Aβ42 fibrils with Akd^{m}Py vesicles, while keeping the concentration of Aβ42 at 10 μM for each measurement. Fluorescence was monitored in a time-dependent manner and the data were fitted to a standard sigmoidal model.

Results and discussion

The design of functional modular building blocks is crucial for the development of smart functional molecular assembly architectures. The scheme of molecular architectonics allows for the custom design of vesicular architectures that can dissipate in response to specific stimuli. The hydrophilic lipophilic balance (HLB) plays a critical role in the formation and disintegration of molecular assembly architectures such as vesicles, and is achieved through the choice and arrangement of specific molecular segments within an amphiphilic structure (modular building blocks).[2,48] To achieve this goal, three pyrene-conjugated Aβ14-23 peptidomimetics, Akd^{c}Py, Akd^{m}Py, and Akd^{n}Py, with kd units at the C-terminus (c), middle (m), and N-terminus (n), respectively, were designed and synthesized (Fig. 1a). The incorporation of a rigid, proteolytically stable, and biocompatible kd unit imparts hydrogen bonding interactions while the pyrene moiety provides required π–π stacking and hydrophobic interactions.[8–10,42,49–51] The presence of a kd unit in Aβ14-23 at specified positions helps overcome limitations faced by linear peptides and other large cyclic peptide-based molecules.[51] The ^{16}KLVFF^{20} segment derived from Aβ42 is well-known for its ability to recognize Aβ42 aggregation.[38,52] Of the three peptidomimetics, Akd^{c}Py and Akd^{m}Py formed homogeneous solutions in aqueous media, while Akd^{n}Py had poor solubility in water and precipitated out. As a result, Akd^{n}Py was eliminated from further studies. These findings suggest that the position of the kd unit in the molecular structure plays an important role in achieving optimum HLB for molecular organization.

Critical aggregation concentration (CAC)

The critical aggregation concentration (CAC) of both amphiphiles was determined by static light scattering (SLS) measurements. In accordance with Rayleigh theory, bigger particles scatter more light than smaller ones, and as a result, the intensity of the scattered light is directly proportional to the particle size.[53] The inherent luminosity of the fluorophore within the amphiphilic structure gradually increases when the concentration of the amphiphile rises up until the CAC threshold. At that point, any subsequent enhancement in the fluorophore concentration will trigger a sudden shift in the fluorescence intensity due to the onset of larger, aggregated particles (specifically, vesicles). The breakpoint of the plot of intensities of scattered signal *versus* concentration of amphiphile in both situations serves as a clear indication of the CAC value for each amphiphile (Fig. S1, ESI‡). The CAC values for Akd^{m}Py and Akd^{c}Py were found to be 36 and 56 μM, respectively, *i.e.*, these are the critical concentrations at which the amphiphile begins to form the molecular assembly architectures (Fig. S1, ESI‡). The molecularly assembled systems exhibited high stability for more than two months. Their aggregation properties were further examined by various microscopy and spectroscopy studies to determine the morphological features and the aggregation mechanism.

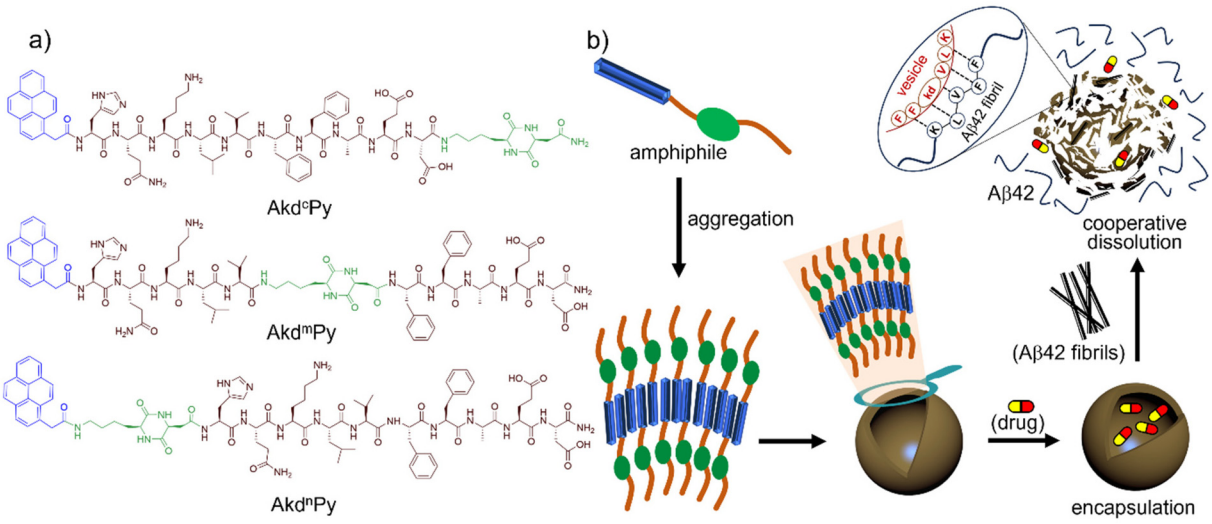

Fig. 1 (a) Chemical structure of synthesized peptidomimetic amphiphiles (Akd^{c}Py, Akd^{m}Py, and Akd^{n}Py); (b) the formation of molecular assembly architecture (vesicle) by peptidomimetic amphiphile (Akd^{m}Py). In amphiphilic structure, the blue segment represents pyrene moiety (hydrophobic segment), the dark brown and green segments represent natural amino acid sequence and unnatural CDP-amino acid (kd) moiety (hydrophilic segment), respectively. The dissipation of drug (Ber) loaded vesicles and dissolution of Aβ42 fibrils is effected through mutual interaction.

Microscopy characterization of Akd^{m}Py and Akd^{c}Py vesicles

The morphology of the molecular assembly formed by Akd^{m}Py and Akd^{c}Py was primarily investigated by TEM study. The TEM data of negatively stained samples confirmed the formation of spherical vesicles with a narrow wall and hollow core. In the case of Akd^{m}Py, the average diameter of the vesicles was (80–100) nm, whereas vesicles with a larger diameter (200–250 nm) were formed by Akd^{c}Py. (Fig. 2a and Fig. S2a, ESI‡). These results were further confirmed by the high-resolution TEM data (Fig. 2b and Fig. S2b, ESI‡). Thus, the formation of vesicular architectures by both the amphiphiles in aqueous media is evident from the TEM data. For further confirmation of the formation of the vesicles by Akd^{m}Py and Akd^{c}Py, FESEM study was performed. The FESEM data for Akd^{m}Py also showed perfectly spherical morphology with an average diameter of 80 nm (Fig. 2c). Similar spherical structures were found in FESEM data of Akd^{c}Py (Fig. S2c, ESI‡). In concurrence with the TEM data, here also the sizes of Akd^{c}Py vesicles were observed in the range of 200–250 nm. AFM study further established the fact that the synthesized amphiphilic molecules (Akd^{m}Py and Akd^{c}Py) have the potential to form the vesicular architecture in aqueous media (Fig. 2d and Fig. S2d, ESI‡). Morphological analysis of AFM data confirmed the formation of spherical vesicles having an average diameter of ~90 nm for Akd^{m}Py (Fig. 2d), while it was ~200 nm for Akd^{c}Py (Fig. S2d, ESI‡). The size distribution of both vesicles was analyzed by use of electron microscopy. Akd^{m}Py vesicles showed an average cross-sectional diameter of 86.5 nm (Fig. 2e), while average diameter size of Akd^{c}Py vesicles was found to be 195.6 nm (Fig. S2e, ESI‡).

DLS study

DLS experiments were carried out to determine the mean hydrodynamic diameter and the size distribution of Akd^{m}Py and Akd^{c}Py vesicles. The size distribution (expressed in number percentage) profiles for both the peptidomimetic amphiphiles with varying concentrations (40–500 μM) were recorded. Here, it was clearly observed that the size distribution for Akd^{m}Py vesicles was in the range of (80–100) nm whereas Akd^{c}Py assembly architectures showed a larger hydrodynamic diameter in the range of (200–250) nm (Fig. 2f and Fig. S2f, ESI‡). More importantly, it is clear from the DLS data that the mean hydrodynamic diameter nearly remains constant as the amphiphile concentrations vary (from 40–500 μM for Akd^{m}Py and from 50–500 μM for Akd^{c}Py), demonstrating the high stability of the vesicles without any concentration-dependent phase alteration. It is also noticed that the DLS data for both synthesized vesicles are in well agreement with the data observed in all the microscopy surveys (Fig. 2 and Fig. S2, ESI‡).

Steady-state fluorescence anisotropy

The microenvironment of any molecular assembly can be investigated by steady-state fluorescence anisotropy measurement. DPH is a most common fluorescence probe used to examine the fluorescence anisotropy (r) for various molecular assembly structures like micelles, vesicles, and bilayers.[17] The r-value was measured for Akd^{m}Py and Akd^{c}Py at their molecularly assembled states over a concentration window of 40–500 μM, which varies in the range of 0.11–0.15 and

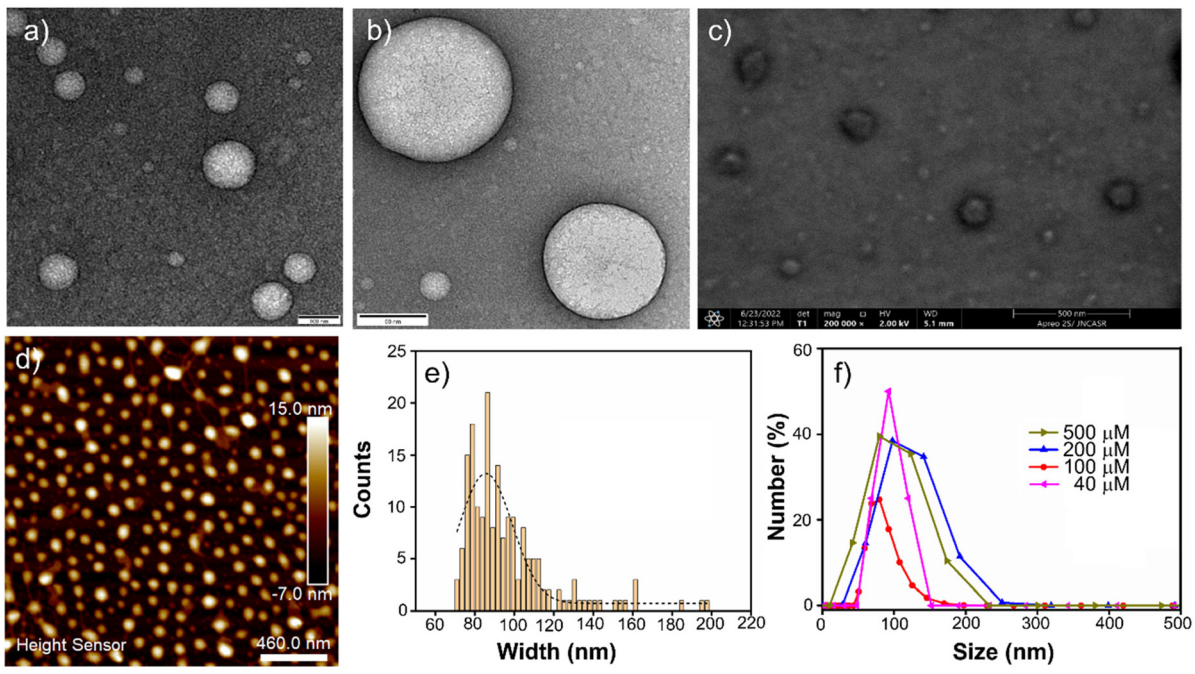

Fig. 2 (a) TEM image, (b) high-resolution TEM image, (c) FESEM image, and (d) AFM image of molecular assembly architectures (vesicles) formed by Akd^{m}Py ([Akd^{m}Py] = 100 μM); (e) size distribution histogram from AFM with a Gaussian fit; (f) concentration-dependent size distribution profile obtained from DLS for Akd^{m}Py vesicle.

Table 1 Steady-state fluorescence anisotropy (*r*) of DPH with varying concentrations of Akd^{m}Py and Akd^{c}Py

Concentration (μM)	*r*-values	
	Akd^{m}Py	Akd^{c}Py
40	0.11	0.09
100	0.12	0.11
200	0.14	0.16
400	0.15	0.16
500	0.15	0.16

0.09–0.16, respectively (Table 1). DPH having rigid, rod-like structure makes itself an ideal membrane fluidity probe that fits easily inside the hydrophobic region of the vesicle. The binding interaction and restricted movement of DPH within the hydrophobic region of aggregated structure cause increase in the anisotropy value. In fact, DPH exhibits greater fluorescence anisotropy for vesicles compared to that of micelles. Interestingly, the observed *r* values of DPH (0.14 for Akd^{m}Py and 0.16 for Akd^{c}Py) are considerably higher compared to that of micellar morphology formed by well-known surfactant, sodium dodecyl sulfate (r = 0.054).[54] The above fact again confirms the formation of stable vesicular architecture by Akd^{m}Py and Akd^{c}Py.

Solvent dependent UV-vis study

At this point, we were keen to understand the molecular level aggregation pattern for the synthesized peptidomimetic amphiphiles (Akd^{m}Py and Akd^{c}Py) that are directed towards the formation of vesicles. From solvent-dependent UV-vis experiments, the aggregation processes of Akd^{m}Py and Akd^{c}Py amphiphiles were examined. In both cases, the solvent composition was varied from DMSO (molecularly dissolved state) to water (molecular assembly state) *via* an intermediate solvent mixture (1 : 1 (v/v) DMSO–water). Interestingly, Akd^{m}Py and Akd^{c}Py both showed blue shifted UV-vis absorption maxima upon moving from a molecularly dissolve state to a molecular assembly state (Fig. 3a and b). The absorption spectra of Akd^{m}Py exhibited the maxima at λ_{max} = 348 nm and this was blue shifted to λ_{max} = 342 nm upon changing the solvent from DMSO to water (Fig. 3a). Similarly, Akd^{c}Py showed blue shifting absorption maxima from λ_{max} = (351–343) nm when the composition of solvent system was varied (Fig. 3b). It is well-known that the blue shifting of absorption peak from a non-assembled state to a molecular assembly state indicates the self-organization of molecules through parallel face-to-face stacking arrangement which forms a sandwich-type pattern

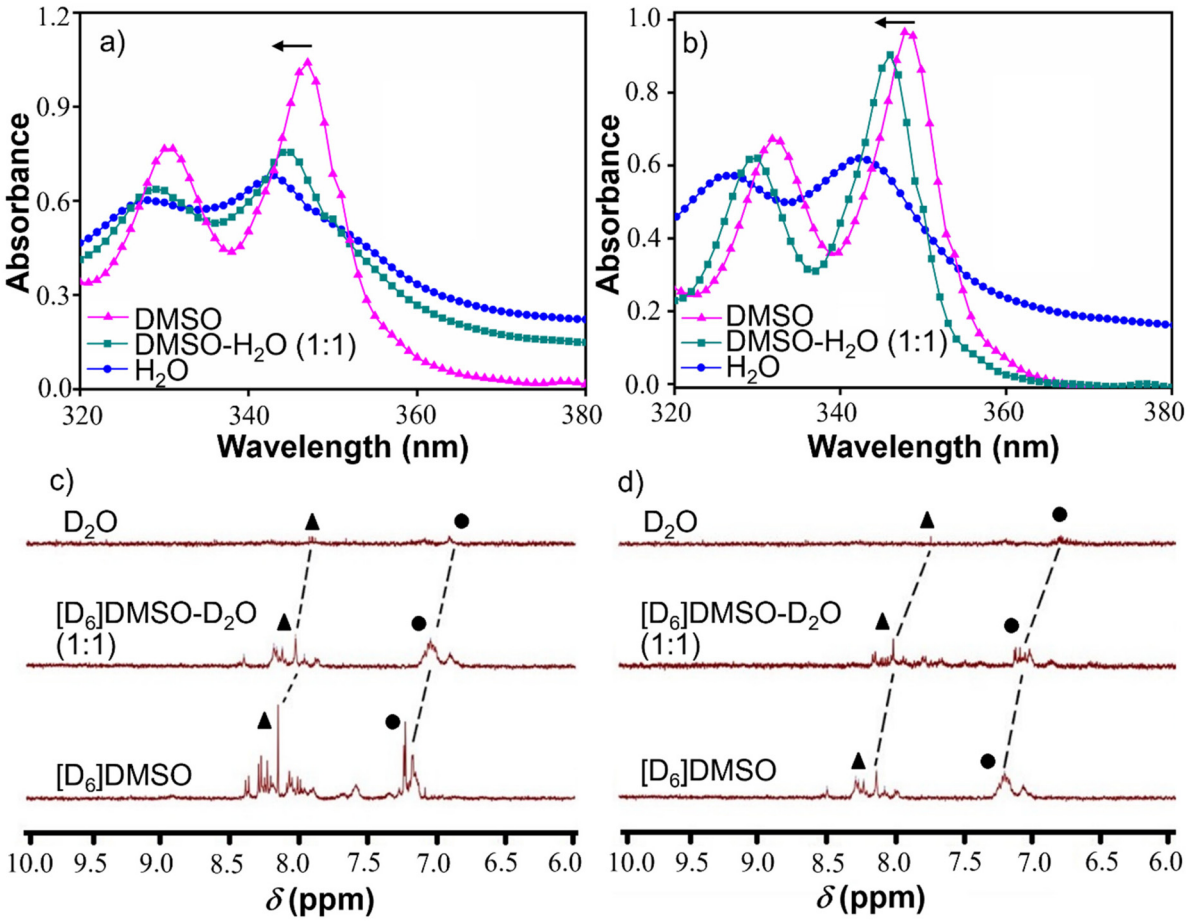

Fig. 3 UV-vis spectra of (a) Akd^{m}Py and (b) Akd^{c}Py in different solvent systems (50 μM) (the arrows indicate the blue shift of absorption spectra in each case); solvent dependent ^{1}H-NMR spectra of (c) Akd^{m}Py and (d) Akd^{c}Py showing the shift of pyrenyl (▲) and L-phenylalanine aromatic protons (●).

termed H-type molecular assembly.[55] The solvent dependent UV-vis absorption studies revealed H-type assembly of Akd^{m}Py and Akd^{c}Py. The mechanism of vesicle formation through H-type stacking of peptidomimetic amphiphile is depicted schematically in Fig. 1b.

Solvent dependent ^{1}HNMR study

The solvent-dependent ^{1}H-NMR experiment was carried out for both peptidomimetic amphiphiles (Akd^{m}Py and Akd^{c}Py) in order to identify the interacting forces that lead to the formation of molecular assembly architectures (vesicle). It is observed that upon transformation from a non-assembled state in DMSO-d_6 to a molecular assembly state in D_2O, the NMR signals of aromatic protons exhibited a gradual upfield shift with decreased peak intensity (Fig. 3c and d). In DMSO-d_6, the pyrenyl aromatic proton of Akd^{m}Py showed sharp peaks at δ = 7.89–8.41 ppm while the aromatic protons of phenylalanine moieties showed distinguished peaks at δ = 7.09–7.26 ppm (Fig. 3c). Akd^{m}Py exists in a molecularly dissolved state in DMSO-d_6. Upon increasing the percentage of D_2O, the peaks shifted to upfield region *i.e.*, at δ = 7.88 ppm and 6.87 ppm, respectively, accompanied with reduced peak intensities (Fig. 3c). These change in chemical shift values further confirms the aggregation behaviour of our synthesized amphiphile. Similarly, the NMR signals of pyrenyl aromatic protons of Akd^{c}Py got upfield shifted form δ = 7.98–8.31 ppm to δ = 7.85 ppm (Fig. 3d) on transforming form molecularly dissolved state (in DMSO-d_6) to molecular assembly state (in D_2O). Notably, the aromatic protons of phenylalanine moieties also exhibited upfield shifting of the NMR signals from δ = 7.01–7.31 ppm to δ = 6.86 ppm (Fig. 3d). Therefore, the self-assembly process of both amphiphiles was observed to occur concomitantly with an increase in D_2O content. Thus, these results delineate the active participation of hydrophobic and π–π stacking interaction during the molecular aggregation of both amphiphiles contributed together to form the vesicular nano-architectures.[18,49]

Dye entrapment and release studies

To further understand the vesicular nanostructure formed by the amphiphiles (Akd^{m}Py and Akd^{c}Py), a dye encapsulation study was performed. This study also confirmed the presence of a hydrophilic compartment inside the vesicles and their ability to encapsulate water-soluble cargo in their inner hydrophilic domain. Rhodamine B (RhB), a water-soluble fluorescent dye, was selected as the model drug. Water soluble RhB can accommodate itself in the inner core of the vesicles. During the process of loading the dye inside the vesicles, the unentrapped RhB was discarded by size exclusion chromatography using sephadex G-25. The eluted solution of entrapped RhB showed a characteristic UV-vis absorbance peak at λ_{max} = 554 nm indicating the presence of the dye within the vesicles (Fig. S3a, ESI‡). Here, we calculated the loading percentage of the entrapped RhB after rupture of vesicles with Triton X-100 solution (0.5% (v/v)). The RhB loading was 75% for Akd^{m}Py vesicles and 71% for Akd^{c}Py vesicles (Fig. S3b, ESI‡) calculated from the standard calibration curve (absorbance *versus* concentration) of RhB. Dye entrapped vesicles (Akd^{m}Py and Akd^{c}Py) were further examined under a fluorescence microscope, which showed red-emitting spheres (Fig. 4a and Fig. S4a, ESI‡), confirming the effective RhB entrapment inside the vesicles. RhB encapsulation was further certified by comparing the fluorescence intensities of free and encapsulated RhB at λ = 578 nm. It was intriguing to note that the fluorescence intensity of vesicle-entrapped RhB was significantly lower than that of only RhB (Fig. S5a and b, ESI‡), maybe as a result of the fluorophore's self-quenching ability under constrained circumstances.[56]

The release of the entrapped dye molecules from the hydrophilic compartment of the vesicles was evaluated by fluorescence spectroscopy. As observed earlier, the emission intensity of entrapped RhB in the Akd^{m}Py vesicle was found to be sufficiently low. Interestingly, upon treatment with Triton X-100, the emission intensity increased significantly and became comparable to that of RhB (Fig. S5a and b, ESI‡). This observation clearly supports the release of dye molecules from the hydrophilic interior of the vesicle into the bulk solvent through the disintegration of the vesicle. Additionally, the fluorescence microscope data showed the dispersed fluorescence signal throughout the sample, indicating that both the vesicles (Akd^{c}Py and Akd^{m}Py) were fragmented and their contents were released (Fig. S4b and c, ESI‡). This is consistent with the earlier finding that the vesicles were disrupted by the detergent (Triton X-100) treatment. This property may have implications for the use of these vesicles in potential therapeutic applications or as tools in cell biology research.

Drug loading and release studies

To utilize the synthesized vesicles as a delivery platform, the neuroprotective drug, Ber, was loaded into Akd^{m}Py vesicles using a traditional thin-film hydration process. Akd^{m}Py vesicles were chosen for drug encapsulation studies due to their appropriate size of 80 nm for cellular transportation or drug delivery, while Akd^{c}Py vesicles were excluded due to their larger size of 200–250 nm. The entrapment of Ber within Akd^{m}Py vesicles was confirmed by fluorescence microscopy data, and release studies were conducted using fluorescence spectroscopy (Fig. S6a, ESI‡). The fluorescence signal for Ber encapsulated within the vesicles was weaker compared to that of unencapsulated Ber (Fig. S6b, ESI‡). However, the signal was restored after treatment of drug loaded vesicles with Triton X-100 (Fig. S6b, ESI‡). The drug loading efficiency was calculated to be 66% from the standard calibration plot (Fig. S6c, ESI‡). These results suggest that Ber can be effectively entrapped within Akd^{m}Py vesicles. Ber is effectively encapsulated in the inner core of the vesicle and thereby it is protected from physiological degradation, which resulted in extended half-life, and subsequent controlled release of drug.[18,57]

Interaction of Akd^{m}Py vesicles with Aβ42 fibrils

Akd^{m}Py is derived from KLVFF, a pentapeptide recognition motif which is known to target Aβ42. The interaction between Aβ42 fibrils and Akd^{m}Py vesicles was investigated by spec-

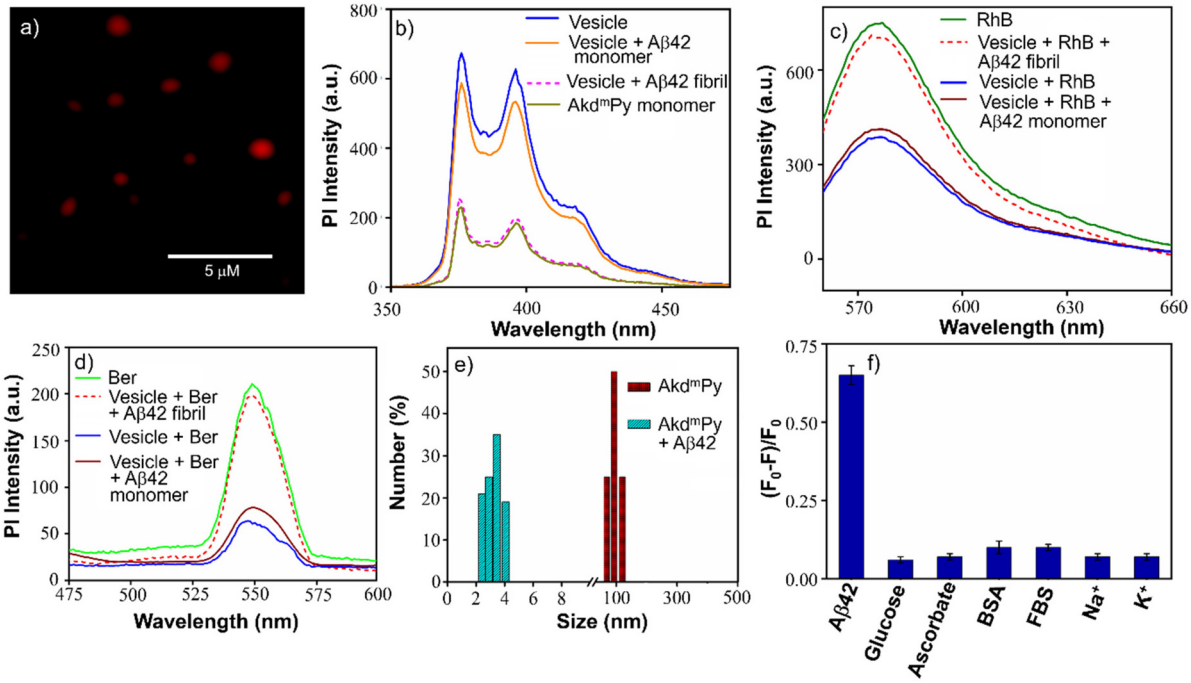

Fig. 4 (a) Fluorescence microscopy image of RhB entrapped within Akd^{m}Py vesicles; (b) fluorescence emission spectra of Akd^{m}Py monomer and molecular assembly of Akd^{m}Py (40 μM) before and after treatment with Aβ42 fibril and Aβ42 monomer (10 μM); (c) fluorescence emission spectra of only RhB and RhB entrapped within Akd^{m}Py vesicle before and after treatment with Aβ42 fibril and Aβ42 monomer (10 μM); (d) fluorescence emission spectra of only Ber and Ber entrapped within Akd^{m}Py vesicle before and after treatment with Aβ42 fibril and Aβ42 monomer (10 μM); (e) size distribution of Akd^{m}Py vesicles before (red) and after (cyan) treatment with Aβ42 fibril; (f) relative change in fluorescence intensity of Akd^{m}Py (40 μM) in the absence and presence of various biologically relevant species (10 μM). Percent errors are within ±5% in triplicate experiments.

troscopy and microscopy techniques. At first, the fluorescence emission of Akd^{m}Py at the monomeric state (10 μM) and at the vesicular state (40 μM) was recorded. The fluorescence intensity of Akd^{m}Py was considerably higher than that of Akd^{m}Py at a monomeric state. It is most likely caused by the presence of the hydrophobic domain of Akd^{m}Py molecular assembly (Fig. 4b). However, the formation of the excimer band for pyrene-containing molecules during the formation of molecular assembly was not observed. This could be attributed to the lack of energetically favourable orientation and close packing of the molecules during molecular assembly process.[58] Interestingly, the addition of preformed Aβ42 fibrils (10 μM) to Akd^{m}Py vesicles resulted in quenching of the fluorescence intensity (Fig. 4b). This further confirms the disintegration of molecular assembly architectures (Akd^{m}Py vesicles) leading to loss of hydrophobic domain[59] which resulted in quenching of the fluorescence. In contrast, there was no significant change found when Akd^{m}Py vesicles in the presence of Aβ42 monomers (Fig. 4b). To further verify the disintegration of Akd^{m}Py vesicle in the presence of Aβ42 fibril, both dye and drug release studies were performed.[18] It was found that the fluorescence intensity increased abruptly and became comparable to that of RhB upon addition of Aβ42 fibrils to the RhB loaded Akd^{m}Py vesicles (Fig. 4c). In contrast, no observable change in fluorescence was observed for dye loaded vesicles in the presence of Aβ42 monomer (Fig. 4c). This result confirmed the dissipation of the vesicles in the presence of Aβ42 fibrils. Similarly, the fluorescence data demonstrated that the addition of Aβ42 fibrils caused the disintegration of drug-loaded Akd^{m}Py vesicles followed by the release of the drug while Aβ42 monomer had no effect (Fig. 4d). Next, the DLS histogram of Akd^{m}Py vesicle showed that upon treatment with Aβ42 fibrils, the peak corresponds to the hydrodynamic diameter of Akd^{m}Py vesicle at ~ 90 nm completely disappeared, which infer the disintegration of vesicles (Fig. 4e). A new peak appeared at around 3–5 nm probably due to small molecular aggregation species of disintegrated vesicles. At this point, the specificity of the interaction between Akd^{m}Py and Aβ42 fibrils was tested. The fluorescence spectra of Akd^{m}Py were recorded in the presence of various biologically relevant species such as glucose, sodium ascorbate, proteins (BSA, FBS), essential metal ions (Na^+, K^+). From the relative intensity of fluorescence spectra, it was confirmed that the interaction of Akd^{m}Py vesicles with these biologically relevant species is negligible compared to that of Aβ42 fibrils (Fig. 4f). KLVFF, the recognition moiety that drive the self-aggregation of Aβ42 peptide is also found in Akd^{m}Py vesicles.[60] Therefore, Akd^{m}Py vesicles directly interact with Aβ42 fibrils with excellent selectivity.[51]

The fate of Aβ fibrils upon interaction with Akd^{m}Py vesicles was investigated by TEM imaging and analysis (Fig. 5a–d). TEM image of untreated Aβ42 showed long matured fibrillar structures (Fig. 5a). In comparison, the dissolution of Aβ42 fibrils had been clearly observed upon addition of Akd^{m}Py

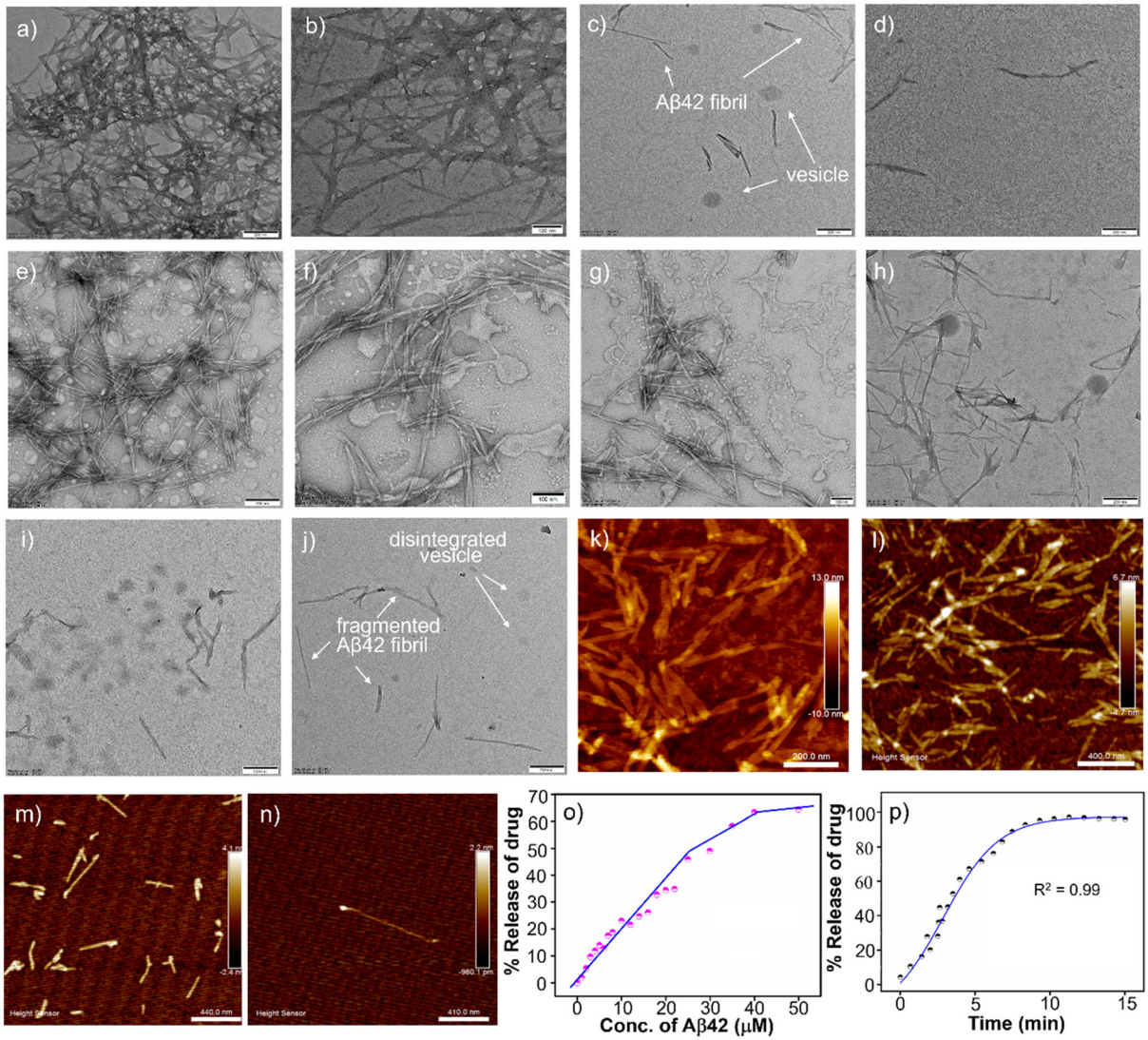

Fig. 5 (a) TEM image of Aβ42 fibrils (10 μM); TEM images of Aβ42 fibrils in the presence of (b) 25 μM, (c) 40 μM and (d) 80 μM of Akd^{m}Py; TEM images of Aβ42 fibrils (10 μM) incubated with Akd^{m}Py vesicle (40 μM) for (e) 5 min, (f) 30 min, (g) 1 h, (h) 6 h, (i) 24 h and (j) 48 h; (k) AFM image of Aβ14-23 fibrils (10 μM); AFM images of Aβ14-23 fibrils in the presence of (l) 25 μM, (m) 40 μM and (n) 80 μM of Akd^{m}Py; (o) percentage release of Ber with an increase in concentration of Aβ42 fibrils; (p) time-dependent release of Ber.

vesicles (Fig. 5b–d). At concentration of Akd^{m}Py amphiphile (25 μM) below CAC (36 μM), the dissolution of Aβ42 fibrils was not effective (Fig. 5b). However, Akd^{m}Py clearly promotes dissolution of Aβ42 fibrils at concentration (40 μM) beyond the CAC (Fig. 5c). As shown in Fig. 5d, at higher concentration (80 μM) of Akd^{m}Py almost complete dissolution of Aβ42 fibrils was observed, which reiterate the potential of Akd^{m}Py vesicles to modulate toxic Aβ42 fibrils. Furthermore, circular dichroism (CD) studies were performed to understand the effect of Akd^{m}Py vesicle on Aβ42 fibril-induced secondary conformations. The negative Cotton effect at 218 nm (−2.1 mdeg) in the CD spectrum of Aβ42 fibrils (10 μM) confirmed aggregation of Aβ42 through the β-sheet conformation (Fig. S7a, ESI‡).[51] After treatment with Akd^{m}Py vesicles (40 μM), the CD spectrum altered suggesting random coil conformation of Aβ42.[61] Thus, CD data confirmed the fact that Akd^{m}Py vesicle has the potential to modulate the secondary conformation of Aβ42 (fibrils) from β-sheet to random coil which resulting in its dissolution.

Next, we investigated the effect of Aβ42 fibrils on Akd^{m}Py vesicles by TEM analysis. Molecular architectures are formed by various weak interactions and their structures can be easily disturbed by external environmental factors and agents.[21] It was anticipated that Aβ42 fibrils could trigger the dissipation of vesicles by the interaction of Aβ42 through KLVFF moiety present on vesicle.[51,52] TEM imaging was performed on preformed Aβ42 fibril (10 μM) samples incubated with Akd^{m}Py vesicles (40 μM) at different time intervals (Fig. 5e–j). After 5 min of incubation, the coexistence vesicles and fibrils were observed (Fig. 5e). Interestingly, at 30 min, the vesicles were found to be distorted and the density of Aβ42 fibrils was reduced (Fig. 5f). This data further confirmed the mutual interaction driven changes to Aβ42 fibrils and Akd^{m}Py vesicles.

Observations after 1 h of incubation revealed the presence of some distorted vesicles and dissolved fibrils (Fig. 5g). As the incubation period of 1 h and beyond (24 h), the vesicular structures were almost entirely absent (Fig. 5h and i). Intriguingly, with incubation time increased, there was a corresponding dissolution of Aβ42 fibrils. At 48 h incubation, all distorted vesicles were further fragmented, and no detectable vesicular architectures was observed (Fig. 5j). From this data, it can be concluded that the Aβ42 fibrils and Akd^{m}Py vesicles mutually interact and disintegrate. The interaction ability of Akd^{m}Py vesicle with Aβ42 fibrils is better than that of Aβ42 recognition (KLVFF) sequence binding interaction (hydrophobic and hydrogen bonding), which is possibly attributed to the large surface area of the vesicles. The change in the optimum HLB of the vesicles during their interaction with Aβ42 fibrils resulted in the dissipation of the former. Therefore, multivalent interactions involving simultaneous engagement of multiple interacting species (between vesicle and Aβ42 fibrils) results in better binding strength and specificity compared to vesicle–vesicle or fibril–fibril interactions.[62]

The structural component of the peptidomimetic amphiphile responsible for the dissolution of Aβ42 fibrils was investigated. The Aβ14-23 peptide was used as a representative model of the Aβ peptide.[51] The AFM data (Fig. 5k–n) corroborated the results observed in previous TEM studies. The AFM images demonstrated the formation of mature fibrils by Aβ14-23 (Fig. 5k). Akd^{m}Py vesicles treated samples showed the dissolution of Aβ14-23 fibrils (Fig. 5l–n). Interestingly, Akd^{m}Py monomer (below CAC) had a minimal effect on the dissolution of Aβ14-23 fibrils. At concentrations above CAC, Akd^{m}Py showed better dissolution effect on Aβ14-23 fibrils (Fig. 5m and n). This study demonstrated that the KLVFF recognition moiety is primarily responsible for the mutual interaction and dissolution of Aβ42 fibrils and Akd^{m}Py vesicles. This observation was further confirmed by CD spectroscopy analysis. The negative cotton band at 218 nm (−9.1 mdeg) in the CD spectra of Aβ14-23 fibrils (10 μM) indicates a β-sheet conformation (Fig. S7b, ESI‡). This band disappeared upon interaction with Akd^{m}Py vesicles (Fig. S7b, ESI‡). Therefore, it can be concluded that the KLVFF moiety present in Akd^{m}Py and Aβ42 plays a crucial role in mutual interaction and dissolution of vesicles and fibrils, respectively.

ThT fluorescence study

To investigate the effect of Akd^{m}Py vesicles in promoting the disaggregation of Aβ42 fibrils, thioflavin T (ThT) assay was performed. The comparative fluorescence intensity of ThT was monitored in a time-dependent manner (0–48 h) in the presence of Akd^{m}Py vesicles and Aβ42 fibrils. With increase in incubation time, a gradual decrease of ThT fluorescence intensity was observed (Fig. S8, ESI‡). The decrease in ThT fluorescence intensity further confirmed the effective dissolution of Aβ42 fibrils.[63]

Aβ42 fibril responsive drug release

The preliminary studies have confirmed the successful encapsulation of the neuroprotective drug, Ber, within the Akd^{m}Py vesicle. The selective disintegration of Akd^{m}Py vesicle was observed in response to Aβ42 fibrils, while similar effect was not observed in the presence of Aβ42 monomers. Drug release study was performed at varying concentrations of Aβ42 fibrils, which showed a concentration-dependent increase in release of Ber, as assessed by the corresponding fluorescence intensity of the released Ber (Fig. 5o). At a concentration of 40 μM of Aβ42 fibrils, up to 70% of the drug was released from Akd^{m}Py vesicles (Fig. 5o). The release of drug molecules resulted due to the dissipation of the vesicles upon interaction with Aβ42 fibrils. Time also plays a significant role in this process. The drug release kinetics showed a sigmoidal nature of the drug release profile. Kinetic analysis inferred to an initial rapid release (up to 8 min) followed by a slow release of Ber (Fig. 5p). It was found that up to 92% of the drug was released within 8 min in the presence of 10 μM of Aβ42 fibrils. Thus, the dissipation of drug-loaded Akd^{m}Py vesicles resulted in effective release of Ber.

Dissolution of Aβ42 fibrils

As established, the misfolding and assembly of Aβ42 into insoluble fibrils and plaques is considered a key characteristic of AD.[22] The potential of drug-loaded Akd^{m}Py vesicles as effective modulators of Aβ42 fibrils was evaluated. The preformed Aβ42

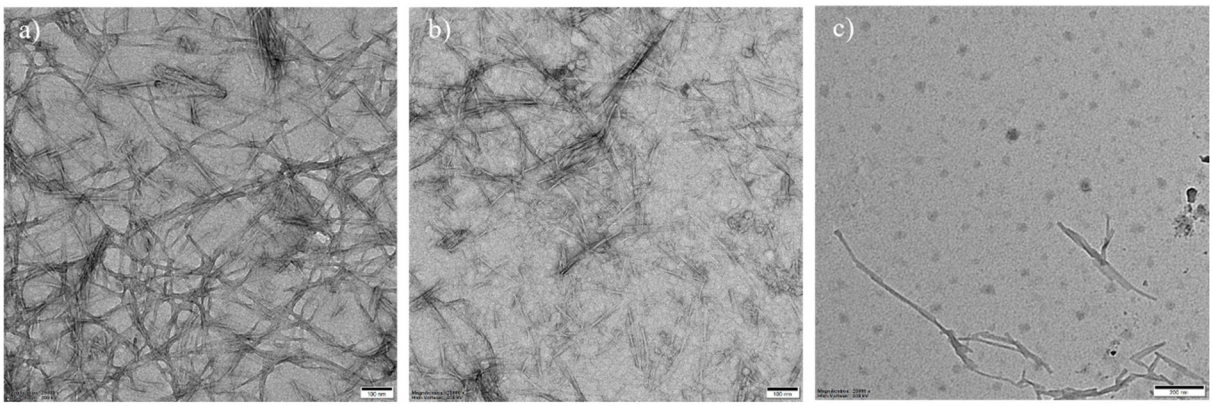

Fig. 6 TEM images of Aβ42 fibrils (10 μM) in the presence of (a) Ber (10 μM) (b) Akd^{m}Py vesicle (40 μM) and (c) Ber loaded (10 μM) Akd^{m}Py vesicle for 1 h.

fibrils (10 μM) were incubated independently with Ber (10 μM), Akd^{m}Py vesicle (40 μM), and Ber (10 μM) loaded Akd^{m}Py vesicles. TEM imaging was performed after 1 h of incubation, and the data was analyzed to determine the effects of drug, vesicle, and drug-loaded vesicle on Aβ42 fibrils. Notable differences in the dissolution of Aβ42 fibrils was observed under these different conditions. There was no significant effect of Ber (10 μM) (Fig. 6a), while Akd^{m}Py vesicles (40 μM) showed moderate impact on the dissolution of Aβ42 fibrils (Fig. 6b), accompanied by dissipation of the vesicles. Interestingly, treatment with Ber-loaded Akd^{m}Py vesicles resulted in the dissolution of Aβ42 fibrils (Fig. 6c). Therefore, the synergistic effect of individual components (Ber and vesicle) in Ber-loaded Akd^{m}Py vesicles was found to be highly effective in dissolution of Aβ42 fibrils.

Conclusion

The design and synthesis of a set of pyrene-conjugated and CDP-based unnatural amino acid-containing Aβ14-23 peptidomimetic amphiphiles has been demonstrated. The molecular assembly of the amphiphiles resulted in the formation of vesicular architecture. This scheme of molecular architectonics facilitated the development of stimuli-responsive Akd^{m}Py vesicles, which can selectively interact with Aβ42 fibrils. The characterization of the vesicles was meticulously performed using various microscopy and spectroscopy techniques. The vesicular architectures were further employed for drug (Ber) encapsulation and dissolution of preformed Aβ42 fibrils. The process of dissolution of Aβ42 fibrils by Akd^{m}Py vesicles was thoroughly investigated, which revealed that the KLVFF moiety present in the molecular structure of Akd^{m}Py plays a significant role in interacting with Aβ42 fibrils. The Akd^{m}Py vesicles loaded with the neuroprotective drug (Ber) dissipated in the presence of Aβ42 fibrils, resulting in the release of the active drug. These findings could have substantial implications for in drug delivery and modulating toxic amyloid aggregates associated with various neurodegenerative disorders.

Author contributions

Conceptualization: SD, and TG; investigation and methodology: SD; synthesis: DG; writing – original draft: SD; writing – review and editing: SD, DG, and TG; resources, funding acquisition, supervision, and project administration: TG.

Conflicts of interest

The authors declare no conflict of interest.

Acknowledgements

The authors thank JNCASR, core grant (CRG/DST 2020/004594), Science and Engineering Research Board (SERB), and Department of Science and Technology (DST), New Delhi, India, for the funding. SD thanks SERB-DST for the fellowship.

References

1 M. B. Avinash and T. Govindaraju, *Acc. Chem. Res.*, 2018, **51**, 414.
2 H. Moorthy, L. P. Datta and T. Govindaraju, *Chem. – Asian J.*, 2021, **16**, 423.
3 B. Roy and T. Govindaraju, *Bull. Chem. Soc. Jpn.*, 2019, **92**, 1883.
4 M. B. Avinash and T. Govindaraju, *Nanoscale*, 2014, **6**, 13348.
5 C. E. Schutt and U. Lindberg, *Anat. Rec.*, 2000, **261**, 198.
6 T. Govindaraju and K. Ariga, *Molecular Architectonics and Nanoarchitectonics*, Springer Nature Series of Nanostructure Science and Technology, Springer Nature, Singapore, 2021.
7 M. Konar and T. Govindaraju, Molecular Architectonics, in *Molecular Architectonics and Nanoarchitectonics*, ed. T. Govindaraju and K. Ariga, Elsevier Ltd., Amsterdam, The Netherlands, 2022, pp. 3–342.
8 K. Pandurangan, B. Roy, K. Rajasekhar, Y. V. Suseela, P. Nagendra, A. Chaturvedi, U. R. Satwik, N. A. Murugan, U. Ramamurty and T. Govindaraju, *ACS Appl. Bio Mater.*, 2020, **3**, 3413.
9 S. Manchineella and T. Govindaraju, *ChemPlusChem*, 2017, **82**, 88.
10 C. Balachandra, D. Padhi and T. Govindaraju, *ChemMedChem*, 2021, **16**, 2558.
11 O. Savsunenko, H. Matondo, S. F. Messant, E. Perez, A. F. Popov, I. Rico-Lattes, A. Lattes and Y. Karpichev, *Langmuir*, 2013, **29**, 3207.
12 C. Boyer and J. A. Zasadzinski, *ACS Nano*, 2007, **1**, 176.
13 S. Dinda, S. Sarkar and P. K. Das, *Chem. Commun.*, 2018, **54**, 9929.
14 J. Lehn, *Science*, 1993, **260**, 1762.
15 P. Walde, *BioEssays*, 2010, **32**, 296.
16 C. C. Evans and J. Zasadzinski, *Langmuir*, 2003, **19**, 3109.
17 E. Soussan, S. Cassel, M. Blanzat and I. Rico-Lattes, *Angew. Chem., Int. Ed.*, 2009, **48**, 274.
18 S. Dinda, M. Ghosh and P. K. Das, *Langmuir*, 2016, **32**, 6701.
19 P. Xing, H. Chen, L. Baia and Y. Zhao, *Chem. Commun.*, 2015, **51**, 9309.
20 D. Mandal, S. Dinda, P. Choudhury and P. K. Das, *Langmuir*, 2016, **32**, 9780.
21 F. Versluis, I. Tomatsu, S. Kehr, C. Fregonese, A. W. J. W. Tepper, M. C. A. Stuart, B. J. Ravoo, R. I. Koning and A. Kros, *J. Am. Chem. Soc.*, 2009, **131**, 13186.
22 Alzheimer's Disease: Recent Findings in *Pathophysiology, Diagnostic and Therapeutic Modalities Royal Society of Chemistry*, ed. T. Govindaraju, 2022.
23 D. J. Selkoe and J. Hardy, *EMBO Mol. Med.*, 2016, **8**, 595.
24 J. Hardy and D. Allsop, *Trends Pharmacol. Sci.*, 1991, **12**, 383.
25 V. L. Villemagne, S. Burnham, P. Bourgeat, B. Brown, K. A. Ellis, O. Salvado, C. Szoeke, S. L. Macaulay,

R. Martins, P. Maruff, D. Ames, C. C. Rowe and C. L. Masters, *Lancet Neurol.*, 2013, **12**, 357.
26 H. Wang, X. X. Xu, Y. C. Pan, Y. X. Yan, X. Y. Hu, R. W. Chen, B. J. Ravoo, D. S. Guo and T. Zhang, *Adv. Mater.*, 2021, **33**, 1.
27 T. Govindaraju and M. Ramesh, *Chem. Sci.*, 2022, **13**, 13657.
28 K. Rajasekhar and T. Govindaraju, *RSC Adv.*, 2018, **8**, 23780.
29 R. L. Nussbaum and C. E. Ellis, *N. Engl. J. Med.*, 2003, **348**, 1356.
30 C. Soto, *Nat. Rev. Neurosci.*, 2003, **4**, 49.
31 K. Rajasekhar, M. Chakrabarti and T. Govindaraju, *Chem. Commun.*, 2015, **51**, 13434.
32 M. Ramesh, K. Rajasekhar, K. Gupta, V. Babagond, D. K. Saini and T. Govindaraju, *Org. Biomol. Chem.*, 2021, **19**, 801.
33 A. Serrano-Pozo, M. P. Frosch, E. Masliah and B. T. Hyman, *Cold Spring Harbor Perspect. Med.*, 2011, **1**, a006189.
34 R. van der Kant and L. S. Goldstein, *Dev. Cell*, 2015, **32**, 502.
35 D. J. Selkoe, *J. Alzheimer's Dis.*, 2001, **3**, 75.
36 Y. H. Liu, B. Giunta, H. D. Zhou, J. Tan and Y. J. Wang, *Nat. Rev. Neurol.*, 2012, **8**, 465.
37 D. Maity, M. Howarth, M. C. Vogel, M. Magzoub and A. D. Hamilton, *J. Am. Chem. Soc.*, 2021, **143**, 3086.
38 K. Rajasekhar, N. Narayanaswamy, N. A. Murugan, G. Kuang, H. Ågren and T. Govindaraju, *Sci. Rep.*, 2016, **6**, 23668.
39 K. Rajasekhar, C. Madhu and T. Govindaraju, *ACS Chem. Neurosci.*, 2016, **7**, 1300.
40 Q. Li, L. Liu, S. Zhang, M. Xu, X. Wang, C. Wang, F. Besenbacher and M. Dong, *Chem. – Eur. J.*, 2014, **20**, 7236.
41 X. Liang, Y. Wang, J. Song, D. Xia, Q. Li and M. Dong, *Colloids Surf., B*, 2022, **216**, 112575.
42 D. Ghosh, M. Konar, T. Mondal and T. Govindaraju, *Nanoscale Adv.*, 2022, **4**, 2196.
43 K. Rajasekhar, S. Samanta, V. Bagoband, N. A. Murugan and T. Govindaraju, *iScience*, 2020, **23**, 101005.
44 K. Zou, Z. Li, Y. Zhang, H. Zhang, B. Li, W. Zhu, J. Shi, Q. Jia and Y. Li, *Acta Pharmacol. Sin.*, 2017, **38**, 157.
45 S. Strandman, A. Zarembo, A. A. Darinskii, P. Laurinmaki, S. J. Butcher, E. Vuorimaa, H. Lemmetyinen and H. Tenhu, *Macromolecules*, 2008, **41**, 8855.
46 A. Shome, T. Kar and P. K. Das, *ChemPhysChem*, 2011, **12**, 369.
47 H. Tamam, J. Park, H. H. Gadalla, A. R. Masters, J. A. Abdel-Aleem, S. I. Abdelrahman, A. A. Abdelrahman, L. T. Lyle and Y. Yeo, *Mol. Pharmaceutics*, 2019, **16**, 2858.
48 A. Azagarsamy, V. Yesilyurt and S. Thayumanavan, *J. Am. Chem. Soc.*, 2010, **132**, 4550.
49 C. Madhu, B. Roy, P. Makam and T. Govindaraju, *Chem. Commun.*, 2018, **54**, 2280.
50 D. Mandal, T. Kar and P. K. Das, *Chem. – Eur. J.*, 2014, **20**, 1349.
51 M. Konar, D. Ghosh, S. Samanta and T. Govindaraju, *RSC Chem. Biol.*, 2022, **3**, 220.
52 L. O. Tjernberg, J. Naslund, F. Lindqvist, J. Johansson, A. R. Karlstrom, J. Thyberg, L. Terenius and C. Nordstedt, *J. Biol. Chem.*, 1996, **271**, 8545.
53 F. Yin, D. Khago, R. W. Martin and C. T. Butts, *PLoS One*, 2021, **16**, 1.
54 D. Khatua and J. Dey, *J. Phys. Chem. B*, 2007, **111**, 124.
55 Y. Dong, B. Xu, J. Zhang, X. Tan, L. Wang, J. Chen, H. Lv, S. Wen, B. Li, L. Ye, B. Zou and W. Tian, *Angew. Chem., Int. Ed.*, 2012, **51**, 10782.
56 S. Lee, H. Chen, C. M. Dettmer, T. V. O'Halloran and S. T. Nguyen, *J. Am. Chem. Soc.*, 2007, **129**, 15096.
57 D. Zucker, D. Marcus, Y. Barenholz and A. Goldblum, *J. Controlled Release*, 2009, **139**, 73.
58 Y. Hong, J. W. Y. Lam and B. Z. Tang, *Chem. Soc. Rev.*, 2011, **40**, 5361.
59 G. E. Dobretsov, T. I. Syrejschikova and N. V. Smolina, *Biophysics*, 2014, **59**, 183.
60 L. O. Tjernberg, J. Näslund, F. Lindqvist, J. Johansson, A. R. Karlström, J. Thyberg, L. Terenius and C. Nordstedt, *J. Biol. Chem.*, 1996, **271**, 8545.
61 K. Matsuo, R. Yonehara and K. Gekko, *J. Biochem.*, 2004, **135**, 405.
62 Z. Xu, S. Jia, W. Wang, Z. Yuan, B. J. Ravoo and D. S. Guo, *Nat. Chem.*, 2019, **11**, 86.
63 M. Biancalana and S. Koide, *Biochim. Biophys. Acta*, 2010, **1804**, 1405.